LA-ICP-MS U—Pb geochronology of wolframite by combining NIST series and common lead-bearing MTM as the primary reference material: Implications for metallogenesis of South China

Yanwen Tang [a,*], Kai Cui [b,*], Zhen Zheng [c], Jianfeng Gao [a], Junjie Han [a], Jiehua Yang [a], Liang Liu [a]

[a] State Key Laboratory of Ore Deposit Geochemistry, Institute of Geochemistry, Chinese Academy of Sciences, Guiyang 550081, China
[b] Civil and Environmental Engineering School, University of Science and Technology Beijing, Beijing 100083, China
[c] School of Earth Sciences and Resources, China University of Geosciences, Beijing 100083, China

ARTICLE INFO

ABSTRACT

Direct dating of W and W—Sn deposits by wolframite is more reliable relatively to gangue mineral and important for understanding their timing and genesis. However, such analysis still lacks of homogeneous wolframite standard recently. Due to containing considerable and variable common lead, and inhomogeneous in different grains, the wolframite sample of MTM, which is a promising candidate reference material proposed by previous studies, is not suitable as a primary standard for wolframite U—Pb dating by LA-ICP-MS using the normal normalization method as zircons. In this contribution, a modified normalization method is established for wolframite U—Pb dating, in which NIST612 or 614 and MTM are used for correction of Pb—Pb and U—Pb ratios, respectively. Wolframite U—Pb dating are performed on the Langcun, Xihuashan, Piaotang, Shamai W or W—Sn deposits and the Baiganhu ore district, the obtained lower intercept ^{206}Pb/^{238}U ages are comparable with the ages from syngenetic molybdenite, cassiterite, muscovite and the genetically related granites, as well as wolframite by water vapor-assisted ns-LA-ICP-MS U—Pb dating method. The results of this analysis demonstrate that the robust age for W mineralization can be determined by LA-ICP-MS U—Pb dating of wolframite using this modified calibration method. Mineralization ages of 125–130 Ma by directly dating of metal minerals for the Langcun W, Jianfengpo Sn and large-size Xianglushan W deposits confirm that there exists an important W—Sn mineralization event in this period. The close temporal and spatial correlation indicates the granites and W-Cu-Mo-Pb-Zn-Sn mineralization have a genetic relationship with each other and are resulted from the same tectonic-magmatic-hydrothermal events during 140 to 120 Ma in South China.

© 2020 International Association for Gondwana Research. Published by Elsevier B.V. All rights reserved.

1. Introduction

As an important strategic metal in the world, W deposits have attracted increasing attention recently. Direct dating of metal deposits by ore minerals is more reliable relatively to gangue minerals and also important for understanding their timing and genesis. However, the previous U—Pb dating of ore minerals mainly rely on thermal ionization mass spectrometer (TIMS), which is time-consuming and may be affected by the presence of U- and/or Pb-rich micro-inclusions or alteration phases (Romer, 2001; Harlaux et al., 2018). Due to high spatial resolution, high efficiency and low cost, laser ablation inductively coupled plasma mass spectrometry (LA-ICP-MS) has been widely used in U—Pb dating of many minerals including zircon, monazite, apatite,

titanite, etc. Recently, cassiterite and wolframite U—Pb dating by LA-ICP-MS method have made a great progress, tens of typical W or W—Sn deposits have been dated accurately (Yuan et al., 2011; Gao et al., 2014; Li et al., 2016b; Zhang et al., 2017; Luo et al., 2019; Deng et al., 2019), and notably, potential matrix-matched standards, i.e., cassiterite AY-4 and wolframite MTM and LB, have been proposed (Yuan et al., 2011; Luo et al., 2019). Though not homogeneous enough, AY-4 has been confirmed as a useful primary standard in cassiterite U—Pb dating (Gao et al., 2014; Li et al., 2016b; Zhang et al., 2017 and this study). However, MTM and LB have not been well evaluated as a primary standard currently. Some MTM grains were obtained and analyzed in our laboratory, due to inhomogeneity and containing considerable and variable common lead, most of them are not suitable to be the external standard to calibrate Pb/Pb and Pb/U ratios simultaneously. In this contribution, a relatively accurate wolframite U—Pb dating method by LA-ICP-MS was established using MTM and NIST 612 or 614 as the external standards in a modified normalization procedure.

* Corresponding authors.
E-mail addresses: tyw_xt@126.com (Y. Tang), cuikai18@126.com (K. Cui).

2. Sample description and preparation

(1) Wolframite sample HG from the Lancun deposit

South China, a world-famous W—Sn metallogenic region, accounts for nearly 58% and 23% of the world's W and Sn reserves and is at the leading position in the world (Fig. 1A and B) (Sheng et al., 2015; Zhou et al., 2018; USGS, 2019). The Qinzhou-Hangzhou metallogenic belt (QHMB, Fig. 1B) is one of the most important granite-related polymetallic belts in south China. In this belt, W, Sn, Cu and Pb—Zn mineralization are mainly occurred at 160–150 Ma (Mao et al., 2011). More-over, the granitic complex is widely distributed in the northeastern QHMB (NE QHMB), several previous studies have mentioned about that, including Anji Gangkou (Xie et al., 2012; Tang et al., 2012, 2013), Kaihua Tongcun (Chen, 2011; Zhu, 2014; Tang et al., 2017a), Linghou (Tang et al., 2017b) and Lizhu (Jia et al., 2013). Recently, a late and im-portant mineralization event at 140–120 Ma has been well recognized and is mainly related to these complex bodies, based on several newly discovered deposits as well as new geochronology studies on minerali-zation and related granites, e.g., the large-size Xianglushan W (125.5 ± 0.7 Ma, molybdenite *Re*—Os dating, Dai et al., 2018a), Zhuxiling large-size W—Mo (140.2 ± 1.5 Ma, molybdenite *Re*—Os dating, Kong et al., 2018), Mugua (142.2 ± 1.2 Ma, zircon U—Pb age of granite, Li et al.,

2013c), Anji medium-sized Gangkou polymetallic (141–134 Ma, molyb-denite Re—Os dating and zircon U—Pb ages of the complex granites, Xie et al., 2012; Tang et al., 2012, 2013) and Anji Langcun medium-sized W deposits (145–131 Ma, zircon U—Pb age of two late units of the Lancun complex, this analysis). In the Anji Langcun deposit, a granitic complex was identified and composed of three units, e.g., monzogranite porphyry, fine-grained granite and granite porphyry (Fig. 2). This deposit is a newly discovered and characterized by vein-veinlet or disseminated ores, which occurs mainly in or near the contact zone between fine-grained granite and granite porphyry (Fig. 2). HG is chosen at −70 m in ZK001 and characterized by a wolframite-scheelite-quartz-pyrite vein in fine-grained granite (Figs. 2 and 3A–C). Based on field relationships, W mineralization has a close spatial and temporal relationship with fine-grained granite and granite porphyry, and thus zircons from them have also been used for U—Pb dating and comparison. In addition, as shown by a hand specimen from the drilling ZK001, granite porphyry is relatively late and intrudes into fine-grained granite (Fig. 2).

(2) Wolframite samples XHS and PT from the Xihuashan and Piaotang deposits

The W—Sn mineralization in Nanling region of China is mainly formed at 160–150 Ma (Mao et al., 2011). The W resources of this
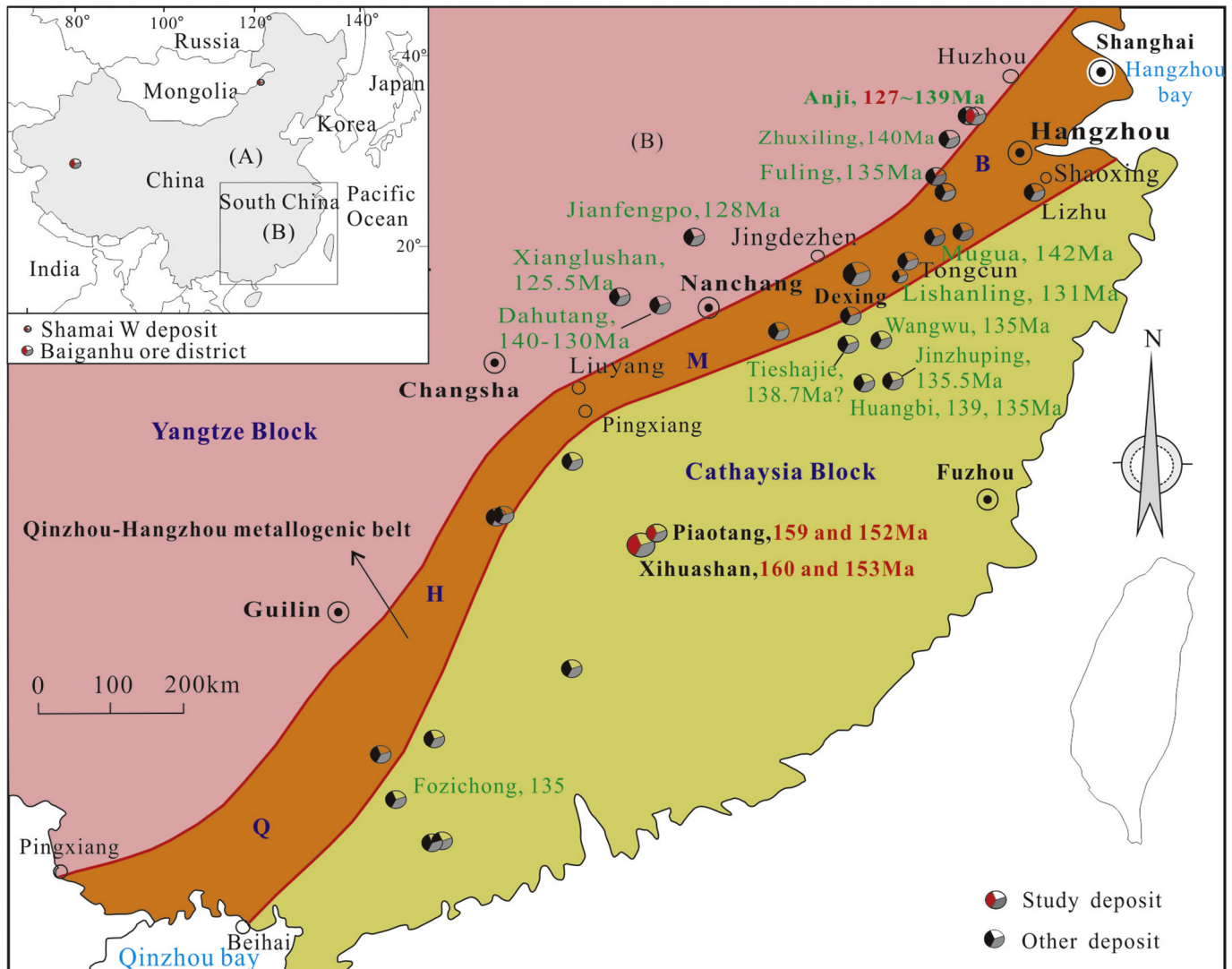

Fig. 1. Location of these W (Sn) deposits in China (A) and especially the Anji Langcun, Piaotang and Xihuashan W (Sn) deposits in South China (B) (modified from Yang and Mei, 1997 and Mao et al., 2011).
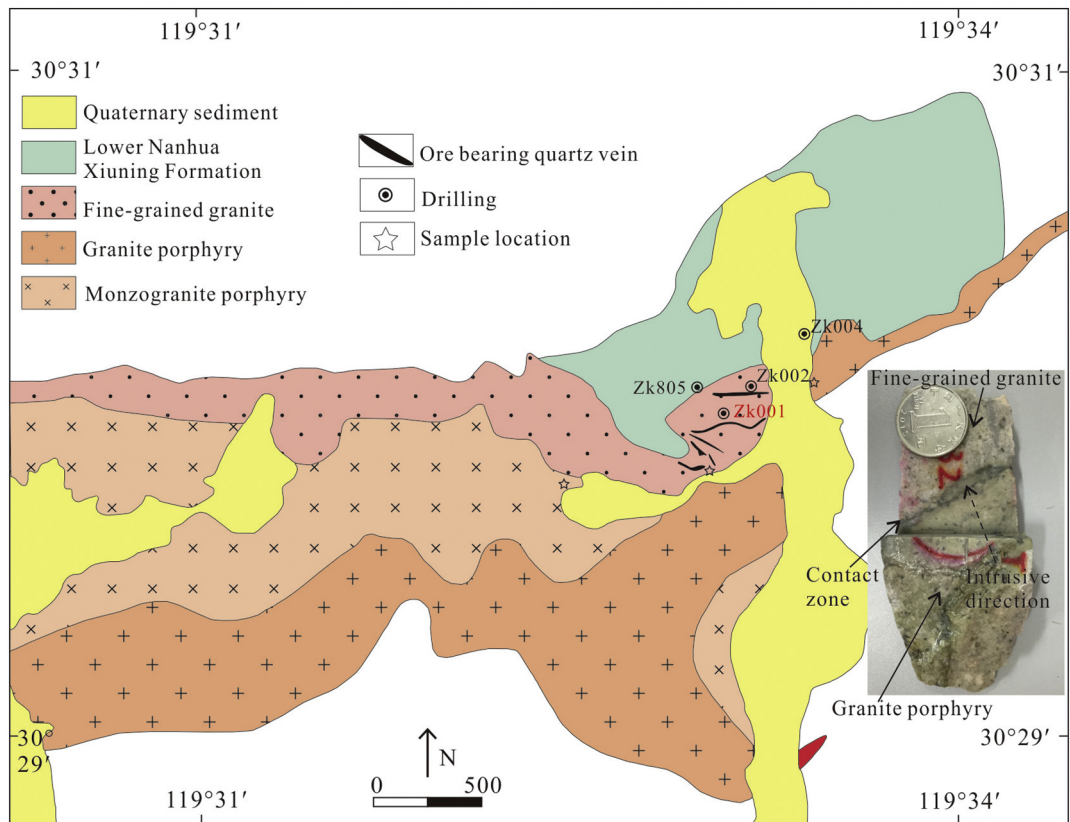
Fig. 2. Geological sketch map of the Langcun W deposit and emplacement relationship between fine-grained granite and granite porphyry (modified from Chen, 2015).

area play a very important role in China as well as the whole world. The Xihuashan and Piaotang are two typical W or W—Sn deposits in this region.

As an important vein-type ore deposit, the Xihuashan tungsten deposit is mainly formed at 157–158 Ma (molybdenite Re—Os dating, Hu et al., 2012 and Wang et al., 2011). The related granitic intrusion belongs to highly fractionated granite, due to high-U contents in zircon, monazite and xenotime are more reliable and yield the ages in the main range of 158–160 Ma (Li et al., 2013a). A late hydrothermal event occurs at 152.8 ± 1.6 Ma (muscovite Ar—Ar, Hu et al., 2012). Sample XHS is from No. 26 ore body at -100 m and intergrowth with quartz, scheelite and minor pyrite (Fig. 3D–F).

The Piaotang W—Sn deposit is dominated by quartz-wolframite veins and has total metal reserves of 91, 800 tons (t) WO₃ (0.154% WO₃ ore grade) and 63, 400 t Sn (0.115% Sn ore grade) (Mao et al., 2013). The ore minerals are mainly wolframite and cassiterite. Cassiterite U—Pb dating constrains the W—Sn mineralization event at 159.5 ± 1.5 Ma (Zhang et al., 2017). Two generations of wolframite have been found and LA-ICP-MS U—Pb dating of them using the water vapor-assisted method has confirmed that the Piaotang deposit is composed by two mineralization events of 159.5 ± 1.3 Ma and 152.1 ± 0.9 Ma (Deng et al., 2019). Mineral assemblage related to wolframite in this deposit has been studied in several previous reports (Zhang et al., 2017; Deng et al., 2019; Yang et al., 2019), and sample PT is from ore body at -268 m and intergrowth with quartz mainly (Fig. 3G–I).

(3) Wolframite sample NM from the Shamai deposit

The Shamai W deposit in the eastern Inner Mongolia, China, is located in the eastern part of the Central Asian Orogenic Belt (Jiang et al., 2016) and is attributed as a greisen and quartz-vein type W deposit (Xie et al., 2015; Jiang et al., 2016; Li et al., 2016a). Wolframite is the major ore mineral and intergrowth with muscovite and quartz (Li

et al., 2016a; Jiang et al., 2016). Muscovite from a wolframite-bearing quartz vein yields an Ar—Ar plateau age of 140 ± 1 Ma (Jiang et al., 2016). Wolframite sample of NM used for U—Pb dating in this analysis is also from the same mineral assemblage (Fig. 3J–L).

(4) Wolframite samples KA-18 and KA-19 from the Baiganhu ore district

The Baiganhu W—Sn ore district, located at the East Kunlun orogenic belt, China, contains total resources of 174, 913 t WO₃ (0.28% ore grade) and 79, 091 t Sn (0.3% ore grade) (Gao et al., 2014). This deposit is primarily characterized by skarn, greisens and quartz-vein type ores (Feng et al., 2013; Gao et al., 2014; Zheng et al., 2016). Minerals in primary mineralization stage mainly include wolframite, cassiterite, muscovite and quartz. The main W—Sn mineralization event has been constrained by cassiterite U—Pb age at 427 ± 13 Ma (LA-MC-ICP-MS, Gao et al., 2014), muscovite ⁴⁰Ar/³⁹Ar ages at 421.8–422.7 Ma (Zheng et al., 2016) or 411.7–412.8 Ma (Feng et al., 2013). LA-ICP-MS and SIMS U—Pb zircon dating of the spatially associated monzogranite yield the ages of 430.5 ± 1.2 Ma (Gao et al., 2014) and 421 ± 3.7 Ma (Li et al., 2012a), respectively. Two wolframite samples (KA-18 and KA-19, Fig. 3M–O) as well as one cassiterite sample (BGH) are all chosen from quartz-vein type ores for dating and comparing with each other. Quartz-vein type ores is often composed by wolframite, cassiterite, quartz, muscovite and minor scheelite (Zheng et al., 2016).

3. LA-ICP-MS U—Pb dating

(1) Wolframite

In order to identify the wolframite internal textures and help to interpret these ages, backscattered electron image (BSE) images of wolframite from these samples were photographed by using a JSM-7800F
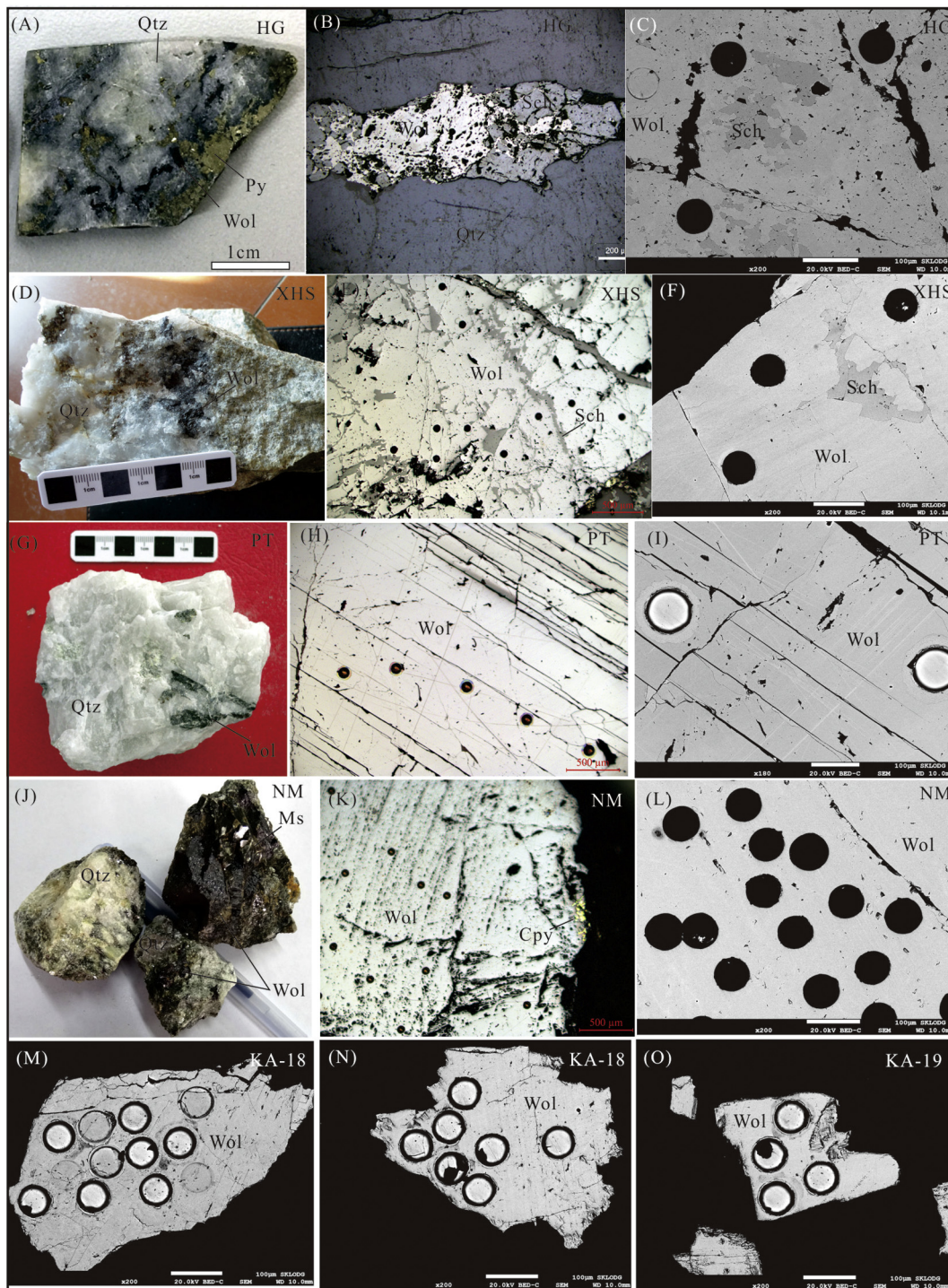
Fig. 3. The occurrence of wolframite samples from the Langcun, Xihuashan, Piaotang, Shamai W (Sn) deposits and the Baiganhu W (Sn) ore district. (A-C) wolframite sample HG, wolframite, scheelite and quartz coexist with each other (reflected light and BSE image) and occur as a vein; (D-F) wolframite sample XHS, wolframite is intergrowth with quartz and scheelite (reflected light and BSE image); (G-I) wolframite sample PT, wolframite is mainly intergrowth with quartz (reflected light and BSE image); (J-L) wolframite sample NM, wolframite is intergrowth with muscovite, quartz and minor chalcopyrite (reflected light and BSE image); (M-O) wolframite grains from KA-18 and KA-19 (BSE image) (Qtz-quartz, Py-pyrite, Wol-wolframite, Ms-muscovite, Sch-scheelite, Cpy-chalcopyrite).

field emission scanning electron microscope at the State Key Laboratory of Ore Deposit Geochemistry (SKLODG), Institute of Geochemistry, Chinese Academy of Sciences (IGCAS), Guiyang, China.

Wolframite U—Pb dating was analyzed by LA-ICP-MS at the SKLODG, IGCAS, Guiyang, China, using an Agilent 7700× ICP-MS equipped with a GeoLasPro 193 nm ArF excimer laser. Analyzed conditions are listed in Table 1. The standard ablation cell was optimized to get a smaller volume and offer faster washout of the aerosol. Before the chamber was closed, the air had been expelled through a helium flow. A laser repetition of 6 Hz, energy density of 5 J/cm^2 and spot size of 60 μm were used for this analysis. The entire content of samples extracted was transported as an aerosol together with helium gas. To

Table 1
Analyzed conditions for LA-ICP-MS measurements.

Geolas Pro 193 nm laser ablation system	
Energy density	5 J/cm^{-2}
Spot size	60 μm
Laser frequency	6 Hz
Ablation cell gas	Helium (0.45 L/min^{-1})
Agilent 7700× ICP-MS	
RF power	~1420 W
Plasma gas flow rate	15.0 L/min^{-1}
Auxiliary gas flow rate	0.93–1.05 L/min^{-1}
Dwell time (ms)	10 ms for ^{202}Hg, ^{204}Pb, ^{208}Pb, ^{232}Th, 100 ms for ^{206}Pb, ^{207}Pb, ^{238}U, and 8 ms for ^{43}Ca, ^{57}Fe, ^{55}Mn, ^{183}W
Addition nitrogen to increases the sensitivity	0–0.3 mL/min^{-1}

increase the sensitivity, small amounts of nitrogen (~3 mL/min) was added to the helium gas via a simple Y junction downstream when the sample aerosol flowed out of the sample cell, and then, argon carrier gas was mixed with them via a T-connector and finally flowed into the ICP-MS (the similar procedure was also described by Hu et al., 2008). Prior to analysis, a steady signal from NIST SRM610 glass was used to optimize mass response and minimize oxide levels. The ThO/Th ratio was typically <0.3% and U/Th ratio was typically at ~1.0. NIST SRM 612 or 614 and an in-house wolframite standard MTM were used as external isotopic calibration standards. MTM was well studied using ID-TIMS with a U—Pb age of 334.4 ± 1.7 Ma (Harlaux et al., 2018) and analyzed as the secondary standard by LA-ICP-MS with the same age using the water vapor-assisted method recently (Luo et al., 2019). The time-dependent drifts of U—Pb isotopic ratios were corrected with a standard-sample bracketing method. NIST612 or 614 was used for mass fractionation correction of Pb—Pb isotope ratios and MTM was used for correction of U—Pb ratios (Similar to the description in Roberts et al., 2017). NIST SRM 612 or 614 was analyzed twice for every ten analyses and MTM was analyzed 5 times for every 7–8 analyses of the tested sample. Additionally, 91500 was analyzed twice every 8–10 analyses during the analysis of wolframite PT. Each spot analysis incorporated a background acquisition of approximately 20 s followed by ~30 s sample data acquisition. To eliminate common Pb contamination from the sample surface, preablation consisted of ~8 pulses of laser ablation was performed in each analysis. In order to preclude the high common lead effect from fluid inclusion or other minerals (e.g., scheelite), only smooth signals were saved. For U—Pb dating analysis, dwell times for each mass scan are 10 ms for ^{202}Hg, ^{204}Pb, ^{208}Pb, ^{232}Th, 100 ms for ^{206}Pb, ^{207}Pb, ^{238}U, and 8 ms for ^{43}Ca, ^{57}Fe, ^{55}Mn, ^{183}W. The data collected from ICP-MS were processed off-line using the ICPMSDataCal software, for calibration, background correction and floating of integration signal. The whole calibration process could be divided as three steps: 1) in the ICPMSDataCal software, choosing NIST612 or 614 as a standard to finish external calibration and time-drift correction, and then exporting and remaining the U, Pb contents, ^{207}Pb/^{206}Pb isotope ratios and uncertainties for use; 2) again in the ICPMSDataCal software, no external calibration and only finishing the time-drift correction, and then exporting and remaining ^{206}Pb/^{238}U isotope ratios and uncertainties for use; and 3) collecting these useful data in excel, calculation the measured ^{238}U/^{206}Pb ratios of MTM and the unknowns, and finishing the correction of this ratios for the unknowns. The final ^{238}U/^{206}Pb(*) values of the unknowns were normalized/multiplied by the accepted/measured ratio of MTM, and the accepted ratio of 18.5–18.7 is from Harlaux et al. (2018) and Luo et al. (2019). Considering the inhomogeneity of different grains of MTM, another in-house wolframite (e.g., NM from Shamai W deposit in here) could be used for quality control and modified the accepted/measured ratio, if necessary. No downhole correction was made for only the first ~25 s ablation

data (excluding the beginning ~2 s) being used in whole process. Isoplot 4.15 was used to calculate the U—Pb ages and draw concordia diagrams. Common Pb correction was employed by a Tera–Wasserburg Concordia or a Tera–Wasserburg Concordia anchored through common Pb (Chew et al., 2011). Then the lower intercept ages can be used as the timing of minerals, e.g., apatite, calcite and wolframtite (Chew et al., 2011; Roberts et al., 2017; Luo et al., 2019). Data errors for isotopic ratios in the following samples are 1 σ.

(2) Zircon

SEM cathodoluminescence (CL) images of zircons from these two samples were photographed by using a JSM-6510 electron microprobe coupled with a Gatan CL Detector at Beijing Geoanalysis Co., Ltd. These images were used to identify zircon internal textures and select target spots for U—Pb dating.

Zircon U—Pb dating was analyzed by LA-ICP-MS at the SKLODG, IGCAS, Guiyang, China, using an Agilent 7900 ICP-MS equipped with a GeoLasPro 193 nm ArF excimer laser. A laser repetition of 6 Hz, energy density of 3 J/cm^2 and spot size of 32 μm were used for this analysis. 91500 was used as the external isotopic calibration standard and was analyzed twice every 8–10 analyses. Plešovice and Qinghu zircons were used for quality control and obtained the consistent age of 338 ± 4.2 Ma (N = 3) and 160.6 ± 2.1 Ma (N = 3), respectively.

(3) Cassiterite

Cassiterite U—Pb dating was analyzed by LA-ICP-MS at the SKLODG, IGCAS, Guiyang, China, using an Agilent 7700× ICP-MS equipped with a GeoLasPro 193 nm ArF excimer laser. AY-4, which has relatively low common lead, was studied using ID-TIMS and LA-ICP-MS methods with a consistent U—Pb age of 158.2 ± 0.4 Ma (Yuan et al., 2011). AY-4 was used as the primary standard during the previous cassiterite U—Pb dating process (Li et al., 2016b; Zhang et al., 2017). In this analysis, AY-4 was also used as external isotopic calibration standard and analyzed four times every 8–10 analyses. An in-house DC cassiterite from Dachang Sn deposit was used for quality control and obtained the intercepts age of 90.4 ± 1.8 Ma (N = 30) in this analysis, similar to the ages from Guo et al. (2018) within the error.

4. Results

4.1. U—Pb isotope data of wolframite

Wolframite U—Pb isotope data for these samples from the Langcun, Xihuashan, Piaotang, Shamai W or W—Sn deposits and the Baiganhu W—Sn ore district are presented in Supp. 1 and described as bellow.

4.1.1. The Langcun W deposit
30 spot analyses on wolframite sample HG have total Pb, Th and U concentrations ranging from 0.3 to 2.9 ppm, 0.1 to 1.7 ppm and 2.0 to 29.9 ppm. A lower intercept ^{206}Pb/^{238}U age of 127.4 ± 4.8 Ma (1σ, MSWD = 1.8) is obtained in Tera-Wasserburg Concordia diagram (Fig. 4a).

4.1.2. The Xihuashan W deposit
Among 19 U-Pb isotope analyses from wolframite sample XHS, most of them have low total Pb (averaging 1.1 ppm), low Th (averaging 0.4 ppm) and moderate U concentrations of 2.0–51.3 ppm (averaging 14.6 ppm). In Tera-Wasserburg Concordia diagram, an obtained lower intercept ^{206}Pb/^{238}U age is 160.9 ± 1.9 Ma (1σ, MSWD = 1.0; Fig. 4b).

4.1.3. The Piaotang W—Sn deposit
28 spot analyses from sample PT have low Th (averaging 0.4 ppm), high U (5.5–65.8 ppm, averaging 32.2 ppm) and relatively high total Pb concentrations of 3.3–10.3 ppm (averaging 4.1 ppm). In Tera-Wasserburg Concordia diagram, these spots obtain a lower intercept ^{206}Pb/^{238}U age of 153.6 ± 1.4 Ma (1σ, MSWD = 2.0; Fig. 4c).
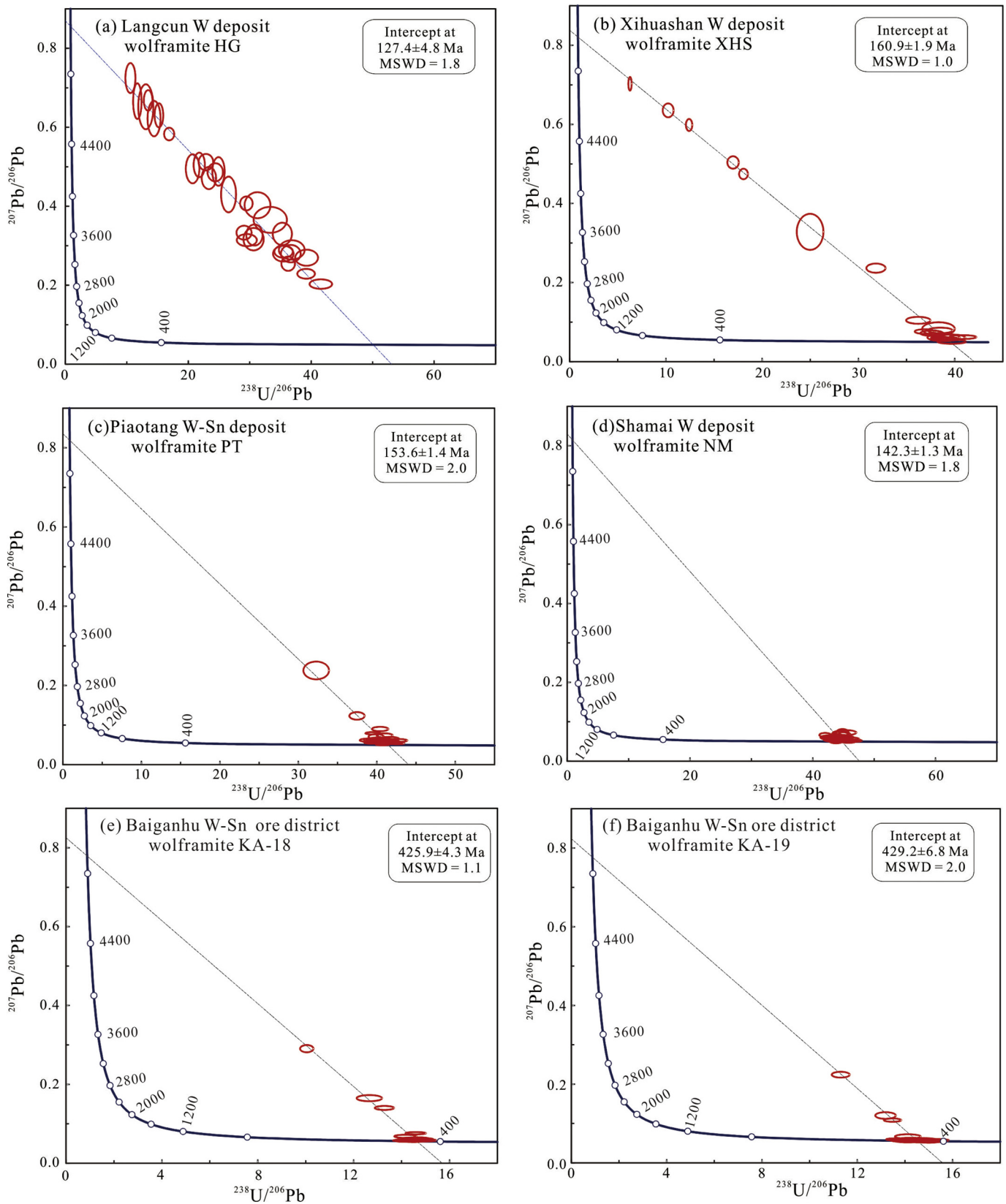
Fig. 4. Tera-Wasserburg plots and the lower intercepts ages of wolframite samples from the Langcun, Xihuashan, Piaotang, Shamai deposits and the Baiganhu ore district (Using NIST612 or 614 and MTM for calibration of Pb–Pb and U–Pb ratios, respectively).

4.1.4. The Shamai W deposit

34 spots are performed on sample NM with low total Pb of 0.4–2.7 ppm (averaging 1.1 ppm), low Th of 0.2–2.1 ppm (averaging 0.7 ppm) and high U of 11.8–136.0 ppm (averaging 47.7 ppm). These spots obtain a lower intercept $^{206}Pb/^{238}U$ age of 142.3 ± 1.3 Ma (1σ, MSWD = 1.8; Fig. 4d) in Tera-Wasserburg Concordia diagram.

4.1.5. The Baiganhu W—Sn ore district

33 spot analyses are performed on wolframite sample KA-18 and KA-19, respectively. 17 spots from each have high U concentrations ranging from 19.6 to 72.9 ppm (averaging 35.2 ppm) and 9.3 to 45.3 ppm (averaging 23.9 ppm), total Pb concentrations ranging from 1.4 to 5.6 ppm (averaging 2.7 ppm) and 0.8 to 5.8 ppm (averaging 1.9 ppm), and Th concentrations ranging from 0.6 to 2.1 ppm and 0.2 to 1.3 ppm, respectively. Two lower intercept $^{206}Pb/^{238}U$ ages of 425.9 ± 4.3 Ma (1σ, MSWD = 1.1; Fig. 4e) and 429.2 ± 6.8 Ma (1σ, MSWD = 2.0; Fig. 4f) are obtained using these 17 spots from each sample in Tera-Wasserburg Concordia diagram, respectively.

4.2. U—Pb isotope data of zircon and cassiterite

Zircon U—Pb isotope data for fine-grained granite and granite porphyry from the Langcun W deposit are presented in Table 2. These zircon grains are euhedral, with the main elongation ratios between 2:1 and 3:1. Most zircons are transparent and colorless under the optical microscope. Oscillatory zonings are common under CL images (Fig. 5a–c). Zircons from fine-grained granite have the U and Th contents of 323–1239 and 225–1029 ppm, respectively, with the Th/U ratios of 0.56–1.29. The older and younger group of zircons from granite porphyry has different U and Th contents (159–1475 and 102–823 ppm, 203–494 and 140–273 ppm, respectively), with the similar Th/U ratios of 0.52–0.84 and 0.55–0.84, respectively. These characteristics show that all zircon grains are of magmatic origin. A total of 30 zircon spots of fine-grained granite were analyzed, of which 21 spots yield a concordant age of 139.5 ± 1.0 Ma and the measured $^{206}Pb/^{238}U$ ratios give a weighted mean age of 139.5 ± 0.7 Ma (MSWD = 1.3) (Fig. 5a). Among 30 zircon spots of granite porphyry, for older group, 19 spots yield a concordant age of 144.0 ± 1.5 Ma and a weighted mean $^{206}Pb/^{238}U$ age of 144.6 ± 1.2 Ma (MSWD = 0.8) (Fig. 5b); for younger group, five spots yield a concordant age of 131.9 ± 2.7 Ma and a weighted mean $^{206}Pb/^{238}U$ age of 131.2 ± 1.8 Ma (MSWD = 0.7) (Fig. 5c).

Twenty-nine analytical spots are measured on more than ten cassiterite grains from the Baiganhu W—Sn ore district. The composition of 28 spots varies from 0.8–29.5 ppm U and 0.1–2.0 ppm total Pb (Table 2). A lower intercept $^{206}Pb/^{238}U$ age in Tera-Wasserburg Concordia diagram and weighted mean $^{206}Pb/^{238}U$ age is 425.6 ± 5.7 Ma (1σ, MSWD = 2.5) and 427.6 ± 5.1 Ma (1σ, MSWD = 2.4) (Fig. 5d), respectively.

5. Discussions

5.1. Comparison and evaluation of results

Among these five deposits, except the Langcun W deposit, many studies have focused on the time of mineralization events and related granites, providing enough data to compare with our analyses.

In the Langcun W deposit, zircon U—Pb isotope data yield a consistent Concordia and weighted mean $^{206}Pb/^{238}U$ age of ~140 Ma (MSWD = 1.3) for fine-grained granite (Fig. 5a), and also yield two consistent Concordia and weighted mean $^{206}Pb/^{238}U$ ages of ~144 Ma (MSWD = 0.7 and 0.8, Fig. 5b), and 131 Ma (MSWD = 0.4 and 0.7, Fig. 5c) for granite porphyry. Zircon spots of three ages are plotted across the Concordia line/curve (Fig. 5a–c), indicating no common Pb was obtained or no radiogenic Pb lost. Moreover, these ages are matched well with granites or the complex in the NE

QHMB (mentioned in sample description). Thus, these three ages are reliable. With regards to two ages for granite porphyry, CL images of two generation zircons have no difference (Fig. 5b,c), indicating that the older zircons are not of inherited cores/zircons origin and more likely to be captured from other intermediate-acid intrusive rock. Moreover, based on field observation, granite porphyry is obviously later than fine-grained granite (Fig. 2). Therefore, the weighted mean age of 131.2 ± 1.8 Ma (MSWD = 0.7) is most likely to represent the formation time of granite porphyry. In addition, a good lower intercept $^{206}Pb/^{238}U$ age of 127.4 ± 4.8 Ma (MSWM = 1.8) (Fig. 4a) is obtained from U—Pb dating of wolframite HG for the Langcun W deposit. This age is consistent with the zircon U—Pb ages of 131 Ma in the error range of LA-ICP-MS method (~4% 2RSD, Li et al., 2015), indicating that W mineralization has a genetic relationship with granite porphyry. This conclusion corresponds with these geological evidences, i.e., W mineralization occurring as veins and cutting fine-grained granite off and granite porphyry intruding into fine-grained granite (Figs. 2 and 3).

In the Xihuashan W deposit, a good lower intercept $^{206}Pb/^{238}U$ age of 160.9 ± 1.9 Ma (Fig. 4b) is obtained from U—Pb dating of wolframite, which agrees well with the molybdenite Re—Os ages (157.8 ± 0.9 Ma and 157.0 ± 2.5 Ma, Hu et al., 2012 and Wang et al., 2011) as well as monazite and xenotime U—Pb ages of the genetically related granite (158–160 Ma, Li et al., 2013a). The Piaotang W—Sn deposit is constrained by wolframite U—Pb age of 153.6 ± 1.4 Ma (Fig. 4c), which is consistent with the second W mineralization event of 152.1 ± 0.9 Ma (Deng et al., 2019).

Wolframite sample NM from the Shamai W deposit has the U—Pb age of 142.3 ± 1.3 Ma (Fig. 4d), which is also consistent with the muscovite Ar—Ar plateau age of 140 ± 1 Ma (Jiang et al., 2016) within error. Wolframite and muscovite are from the same mineral assemblage, indicating that W mineralization in this deposit most likely occurred in the late Jurassic period.

In the Baiganhu W—Sn ore district, wolframite KA-18 and KA-19 have obtained the age of 425.9 ± 4.3 Ma (Fig. 4e) and 429.2 ± 6.8 Ma (Fig. 4f), respectively. Cassiterite (BGH) U—Pb dating in our analysis yields a lower intercept $^{206}Pb/^{238}U$ ages of 425.6 ± 5.7 Ma and a weighted mean $^{206}Pb/^{238}U$ age of 427.6 ± 5.1 Ma (Fig. 5d). These ages agree well with each other and fall in the age range of 412–427 Ma for W—Sn mineralization from previous studies (cassiterite U—Pb and muscovite $^{40}Ar/^{39}Ar$ dating, Feng et al., 2013; Gao et al., 2014; Zheng et al., 2016) and are also confirmed by the age of 421 ± 3.7 Ma (Li et al., 2012a) and 430.5 ± 1.2 Ma (Gao et al., 2014) from the spatially associated monzogranite.

Summarily, the U—Pb ages of wolframite from these deposits are comparable with the ages from syngenetic molybdenite, cassiterite, muscovite and the genetically related granites, as well as wolframite by water vapor-assisted ns-LA-ICP-MS U—Pb dating method. Therefore, these results demonstrate that robust age can be determined for W mineralization by LA-ICP-MS U—Pb dating of wolframite in this calibration method.

5.2. Calibration method

Three calibration methods mainly exist for in situ U—Pb geochronology analysis by LA-ICP-MS attributing to use the different primary standard for the unknown: 1) the same mineral (matrix-matched); 2) the different mineral or NIST glasses (non-matrix-matched); and 3) combining NIST glasses or the different mineral with the same mineral (non-matrix plus matrix-matched).

As a basic calibration method, the same well-characterized natural reference materials for the unknown could improve the quality of LA-ICP-MS U—Pb dating. Thus, many scholars have engaged in searching for matrix-matched standards for dating (Aleinikoff et al., 2007; Kennedy et al., 2010; Li et al., 2012b; Li et al., 2013b; Chew et al., 2014; Gonçalves et al., 2016; Thompson et al., 2016; Roberts et al.,

Table 2
LA-ICP-MS U—Pb isotope data of zircon from the Langcun deposit and cassiterite from the Baiganhu ore district.

Spot No.	Pb	Th	U	Th/U	$^{207}Pb/^{206}Pb$ Ratio	1σ	$^{207}Pb/^{235}U$ Ratio	1σ	$^{206}Pb/^{238}U$ Ratio	1σ	$^{207}Pb/^{206}Pb$ Age(Ma)	1σ	$^{207}Pb/^{235}U$ Age(Ma)	1σ	$^{206}Pb/^{238}U$ Age(Ma)	1σ
	ppm															
Zircons, fine-grained granite, Langcun deposit																
4-01	21	578	802	0.72	0.04943	0.00086	0.14389	0.00245	0.02110	0.00017	169	41	137	2	135	1
4-04	11	331	373	0.89	0.04964	0.00123	0.14794	0.00378	0.02160	0.00025	189	57	140	3	138	2
4-05	35	1029	1239	0.83	0.05054	0.00121	0.15454	0.00347	0.02217	0.00021	220	56	146	3	141	1
4-06	13	490	424	1.15	0.04988	0.00105	0.15311	0.00347	0.02223	0.00026	191	50	145	3	142	2
4-08	21	556	774	0.72	0.05030	0.00110	0.15038	0.00326	0.02168	0.00023	209	45	142	3	138	1
4-09	16	406	606	0.67	0.05011	0.00100	0.15065	0.00318	0.02178	0.00025	211	51	142	3	139	2
4-10	14	327	532	0.61	0.04871	0.00101	0.14939	0.00352	0.02218	0.00026	200	53	141	3	141	2
4-11	21	870	672	1.29	0.04854	0.00106	0.14746	0.00355	0.02200	0.00026	124	52	140	3	140	2
4-12	20	604	746	0.81	0.04934	0.00106	0.14637	0.00316	0.02147	0.00015	165	45	139	3	137	1
4-15	17	424	605	0.70	0.04942	0.00085	0.15086	0.00267	0.02210	0.00019	169	39	143	2	141	1
4-16	20	604	749	0.81	0.04818	0.00077	0.14335	0.00233	0.02159	0.00021	109	34	136	2	138	1
4-17	20	512	721	0.71	0.04869	0.00071	0.14840	0.00241	0.02210	0.00023	132	35	141	2	141	1
4-18	15	363	563	0.64	0.04788	0.00086	0.14616	0.00290	0.02212	0.00023	100	75	139	3	141	1
4-19	18	393	697	0.56	0.04787	0.00086	0.14513	0.00264	0.02202	0.00023	100	72	138	2	140	1
4-20	24	676	883	0.76	0.04790	0.00076	0.14568	0.00271	0.02205	0.00026	95	37	138	2	141	2
4-21	21	541	774	0.70	0.04678	0.00096	0.14178	0.00294	0.02197	0.00018	39	48	135	3	140	1
4-22	25	738	901	0.82	0.04688	0.00083	0.14064	0.00265	0.02174	0.00020	43	41	134	2	139	1
4-23	19	487	719	0.68	0.04785	0.00121	0.14121	0.00296	0.02143	0.00021	100	59	134	3	137	1
4-24	20	540	732	0.74	0.04968	0.00104	0.14925	0.00319	0.02181	0.00022	189	48	141	3	139	1
4-25	9	225	323	0.70	0.04675	0.00110	0.14172	0.00352	0.02201	0.00024	35	65	135	3	140	2
4-28	21	563	770	0.73	0.04841	0.00074	0.14686	0.00233	0.02201	0.00020	120	35	139	2	140	1
4-29	25	674	909	0.74	0.04870	0.00071	0.14604	0.00234	0.02174	0.00021	132	35	138	2	139	1
Zircons (older), granite porphyry, Langcun deposit																
9-01	7	166	288	0.57	0.06276	0.01000	0.16072	0.01680	0.02170	0.00070	702	345	151	15	138	4
9-02	21	605	723	0.84	0.05227	0.00207	0.16346	0.00636	0.02275	0.00029	298	88	154	6	145	2
9-03	6	127	231	0.55	0.05116	0.00660	0.13999	0.01475	0.02284	0.00061	256	265	133	13	146	4
9-06	20	575	685	0.84	0.05209	0.00307	0.15797	0.00839	0.02243	0.00034	300	135	149	7	143	2
9-07	17	349	588	0.59	0.05445	0.00255	0.17601	0.00833	0.02341	0.00034	391	110	165	7	149	2
9-10	9	195	321	0.61	0.05132	0.00433	0.15884	0.01241	0.02292	0.00037	254	192	150	11	146	2
9-13	7	174	256	0.68	0.04988	0.00398	0.14897	0.01056	0.02255	0.00039	191	174	141	9	144	2
9-14	4	102	159	0.64	0.05405	0.00756	0.15315	0.01301	0.02235	0.00048	372	238	145	11	142	3
9-15	5	108	185	0.58	0.04746	0.00488	0.13826	0.01089	0.02233	0.00054	72	226	131	10	142	3
9-16	7	152	231	0.66	0.05240	0.00418	0.16468	0.01094	0.02292	0.00046	302	183	155	10	146	3
9-18	7	148	253	0.58	0.04724	0.00374	0.14703	0.00933	0.02297	0.00044	61	178	139	8	146	3
9-20	26	611	936	0.65	0.05401	0.00448	0.16532	0.01274	0.02230	0.00041	372	187	155	11	142	3
9-22	15	349	549	0.64	0.04657	0.00295	0.14916	0.00954	0.02282	0.00033	33	139	141	8	145	2
9-23	8	164	305	0.54	0.04839	0.00394	0.15024	0.01059	0.02295	0.00045	120	178	142	9	146	3
9-24	6	133	230	0.58	0.05839	0.00524	0.16499	0.01166	0.02279	0.00053	543	192	155	10	145	3
9-25	8	195	283	0.69	0.04933	0.00377	0.14749	0.00950	0.02284	0.00046	165	167	140	8	146	3
9-28	14	276	532	0.52	0.05583	0.00593	0.17286	0.01512	0.02299	0.00058	456	237	162	13	147	4
9-29	38	823	1475	0.56	0.05063	0.00180	0.15716	0.00556	0.02248	0.00027	233	83	148	5	143	2
9-30	5	134	191	0.70	0.04829	0.00636	0.13532	0.01510	0.02193	0.00052	122	276	129	14	140	3
Zircons (younger), granite porphyry, Langcun deposit																
9-12	6	148	231	0.64	0.05392	0.00363	0.14135	0.00739	0.02020	0.00032	369	156	134	7	129	2
9-05	11	261	462	0.57	0.04990	0.00237	0.13941	0.00616	0.02050	0.00029	191	111	133	5	131	2
9-08	12	273	494	0.55	0.05171	0.00253	0.14466	0.00648	0.02056	0.00025	272	111	137	6	131	2
9-11	5	140	203	0.69	0.04556	0.00408	0.12848	0.00989	0.02094	0.00042			123	9	134	3
9-09	7	210	249	0.84	0.05185	0.00442	0.14448	0.00984	0.02094	0.00045	280	192	137	9	134	3
Cassiterite, Baiganhu ore district																
01	0.1	0.0	1.4		0.14071	0.02095	1.42426	0.20259	0.07036	0.00224	2236	260	899	85	438	14
02	1.2	0.0	19.1		0.05693	0.00751	0.55191	0.06985	0.06582	0.00145	487	299	446	46	411	9
03	0.1	0.0	1.7		0.08866	0.01312	0.88320	0.12615	0.06776	0.00214	1398	287	643	68	423	13
04	0.1	0.0	2.2		0.04820	0.00730	0.45372	0.06670	0.06538	0.00184	109	322	380	47	408	11
05	0.2	0.0	2.2		0.05350	0.00798	0.50461	0.07233	0.06624	0.00167	350	307	415	49	414	10
06	0.1	0.0	1.2		0.07677	0.01083	0.71503	0.10410	0.06403	0.00203	1117	284	548	62	400	12
07	0.1	0.0	0.9		0.04879	0.01059	0.46829	0.10018	0.06920	0.00228	200	389	390	69	431	14
08	0.3	0.0	4.9		0.06625	0.00737	0.61945	0.06658	0.06585	0.00135	813	235	490	42	411	8
09	0.3	0.0	5.1		0.05975	0.00599	0.56220	0.05502	0.06586	0.00126	595	219	453	36	411	8
10	0.3	0.0	4.2		0.05687	0.00578	0.55673	0.05510	0.06667	0.00134	487	221	449	36	416	8
11	0.1	0.0	1.0		0.09855	0.01186	0.89895	0.10417	0.06618	0.00233	1598	226	651	56	413	14
12	0.1	0.0	1.1		0.02835	0.00674	0.28894	0.06531	0.06728	0.00218			258	52	420	13
13	0.3	0.0	5.0		0.05648	0.00436	0.53294	0.04082	0.06628	0.00106	472	168	434	27	414	6
14	0.1	0.0	1.6		0.07045	0.00691	0.65915	0.06414	0.06737	0.00134	943	202	514	39	420	8
15	0.1	0.0	1.5		0.06872	0.00804	0.60425	0.06774	0.06525	0.00155	900	244	480	43	407	9
16	0.2	0.0	2.5		0.07938	0.00866	0.78236	0.08510	0.07106	0.00168	1183	217	587	49	443	10
17	0.2	0.0	3.0		0.05324	0.00478	0.51142	0.04406	0.07043	0.00130	339	206	419	30	439	8
18	0.1	0.0	1.0		0.07125	0.00883	0.73594	0.08996	0.07565	0.00225	965	256	560	53	470	14
19	0.1	0.0	1.1		0.05743	0.00862	0.55414	0.08280	0.07263	0.00210	509	335	448	54	452	13
21	1.5	0.0	23.6		0.05626	0.00346	0.54097	0.03273	0.06912	0.00077	461	137	439	22	431	5
22	0.2	0.0	2.7		0.06128	0.00626	0.58311	0.05840	0.06928	0.00124	650	220	467	38	432	8
23	0.9	0.0	13.1		0.05965	0.00425	0.58585	0.04174	0.07046	0.00093	591	156	468	27	439	6

Table 2 (*continued*)

Spot No.	Pb	Th	U	Th/U	$^{207}Pb/^{206}Pb$		$^{207}Pb/^{235}U$		$^{206}Pb/^{238}U$		$^{207}Pb/^{206}Pb$		$^{207}Pb/^{235}U$		$^{206}Pb/^{238}U$	
	ppm				Ratio	1σ	Ratio	1σ	Ratio	1σ	Age(Ma)	1σ	Age(Ma)	1σ	Age(Ma)	1σ
24	0.1	0.0	1.4		0.06411	0.00883	0.59675	0.07343	0.06995	0.00198	746	290	475	47	436	12
25	1.1	0.0	17.1		0.05822	0.00443	0.57064	0.04346	0.07014	0.00096	539	169	458	28	437	6
26	0.1	0.0	1.9		0.06772	0.00780	0.67830	0.07930	0.07060	0.00168	861	236	526	48	440	10
27	0.1	0.0	0.8		0.08431	0.01269	0.81299	0.11548	0.07291	0.00213	1300	296	604	65	454	13
28	0.1	0.0	0.9		0.08078	0.01253	0.72900	0.10866	0.07104	0.00203	1217	309	556	64	442	12
29	0.9	0.0	13.4		0.06034	0.00567	0.59512	0.05595	0.07049	0.00122	617	204	474	36	439	7
30	1.0	0.0	14.5		0.05996	0.00596	0.58794	0.05812	0.07003	0.00124	611	217	470	37	436	8

2017). However, such reference minerals are difficult to find because of these special requirements summarized in previous studies (Li et al., 2013b; Thompson et al., 2016; Roberts et al., 2017), e.g., bearing low common lead (far <1 ppm), having the radiogenic Pb of >98%, virtual isotopic homogeneity, having an abundant source, having the similar composition and ablation characteristics with the unknown, etc. For some inhomogenous reference materials, previous studies have observed that minor variations in composition or/and crystallinity will affect precisely matching between the unknowns and standard materials, and further affect the calculated Pb/U ratios and ages (Black et al., 2004; Thompson et al., 2016). Thus, the well-calibrated natural minerals are still fundamental and desirable for accurate in situ U—Pb dating.

Attributing to the different ablation behavior, significant matrix effects have been observed when non-matrix-matched minerals/materials were used as the reference material for calibrations. Thus, matrix effects are considered to be the major limitations of in situ U—Pb geochronology analysis (Li et al., 2010; Burn et al., 2017). Recently, non-matrix matched calibrations have several successful applications in LA-ICP-MS analysis, e.g., NIST 610, NIST 612 and zircon 91500 as an external standard for allanite and cassiterite U—Pb geochronology, respectively (Yuan et al., 2011; Mcfarlane, 2016; Cheng et al., 2019); a approach of non-matrix-matched standardization has applied in allanite Th-U-Pb dating (Burn et al., 2017); and water vapor-assisted method for U—Pb geochronology of wolframite (Luo et al., 2019). However, owing to the attribute of silicate glass and/or the special laser ablation conditions, e.g., controlling the $^{206}Pb/^{238}U$ ratio at ~0.22 (Cheng et al., 2019), LA-ICP-MS U—Pb dating of accessory minerals seldom use NIST series as the external standard for isotope calibration. Moreover, the widespread application of non-matrix-matched standardization is also limited by its relative uncontrollability, e.g., the matrix dependent downhole fractionation is empirically quantified and corrected (Burn et al., 2017). The water vapor-assisted method may have a great potential to solve the matrix effect problems in LA-ICP-MS U—Pb dating. However, it increases the ThO/Th ratio as high as 0.87% (Luo et al., 2019), which affects determining of trace elements and age simultaneously if necessary. In addition, the newly developed femtosecond (fs)-LA has reduced the matrix effects by half, but cannot eliminate it completely (Zhang et al., 2013; Wohlgemuth-Ueberwasser and Jochum, 2015).

Because of containing common lead and the lack of isotopically homogeneous natural reference material/mineral, the method of combining NIST614 or 612 glass with calcite WC-1 has been widely used in LA-ICP-MS U—Pb dating of calcite or carbonate (Coogan et al., 2016; Roberts and Walker, 2016; Roberts et al., 2017; Nuriel et al., 2017; Godeau et al., 2018). Though what percent of the homogeneity of reference material/mineral can use this method is still unclear, this method has an opportunity to be applied to in situ U—Pb dating of other kinds of ore minerals, e.g., wolframite.

Recently, only wolframite samples of MTM and LB have been reported as the candidate reference materials (Harlaux et al., 2018; Luo et al., 2019). Up to now, no successful U—Pb dating results were reported using them as the calibration materials. The isotopic composition of MTM falls along a mixing line between initial common Pb and

radiogenic components in previous studies (Luo et al., 2019), thus U—Pb normalization can be achieved with this material (Chew et al., 2014; Roberts et al., 2017).

The previous study had confirmed that a much younger lower intercept age will be obtained using zircon 91500 as the external standard for wolframite MTM (Luo et al., 2019), though two relatively large spot sizes of 160 and 90 μm were used. In our comparison analysis, wolframite PT and MTM have obtained lower intercept age of 146.8 and 273.7 Ma (Fig. 6, Supp. 2), respectively, which are both younger than the reported value from Harlaux et al. (2018) and Luo et al. (2019). These results confirmed that 91500 cannot be used as an external standard for wolframite during LA-ICP-MS U—Pb dating due to existing significant matrix effects.

In addition, we performed about twenty spots on MTM grains during the each bracketing analysis section, whereas unexceptionally only a few spots of them have a relatively suitable concordance (≥87%) and be used as primary standard for U—Pb dating of wolframite from these five deposits (Supp. 3 and Fig. 7). These results show that about 13 Ma younger age for the Langcun deposit (Fig. 7a), a much older age (>10 Ma) has obtained for the Xihuashan, Piaotang and Baiganhu (KA-18) deposits (Fig. 7b, c and e), respectively, and a little older but acceptable age for both of the Shamai and Baiganhu (KA-19) deposits (Fig. 7d and f), whereas KA-19 has the larger MSWD value of 4.0 (Fig. 7f). As we known that 91500 is very homogeneous and possesses the common-lead as low as 0.01–0.09 ppm (radiogenic lead>13.0 ppm) (Wiedenbeck et al., 1995). Moreover, each of these selected MTM spots (being the standards in Supp. 3) has the nearly concordant $^{207}Pb/^{235}U$ and $^{206}Pb/^{238}U$ ages, indicating they also contain very low common lead. Thus, the wide range of and high discordance between the $^{207}Pb/^{235}U$ and $^{206}Pb/^{238}U$ ages of other MTM are not likely attributed to calibration process but to containing considerable and variable common lead (not excluding the effect from inhomogeneous distribution of U). Unexpectedly, five wolframite samples were still obtained the uncontrollable U—Pb dating results by using these selected MTM as external standards (Supp. 3). Therefore, it seems that most of MTM grains are not suitable to be external standards to calibrate the Pb/Pb and Pb/U ratios simultaneously.

In contrast, the non-matrix plus matrix-matched calibration method has obtained more robust ages for wolframite U—Pb dating (Supp. 1 and Fig. 4). During this method, the higher $^{238}U/^{206}Pb$ ratio of the samples will obviously improve the quality of the lower intercept $^{206}Pb/^{238}U$ age.

5.3. Implications for understanding the tectonic-magmatic-hydrothermal mineralization event in South China

In South China, the tectonic environment transition from compression to extension during the Late Jurassic to Early Cretaceous (from ~140 to 135 Ma) has been noticed and confirmed by many geologists (Lapierre et al., 1997; Mao et al., 2011; Li et al., 2013c; Lv et al., 2017). And then, in extensional environment, numerous A-type granites were identified from 140 to 120 Ma in or near the NE QHMB of South
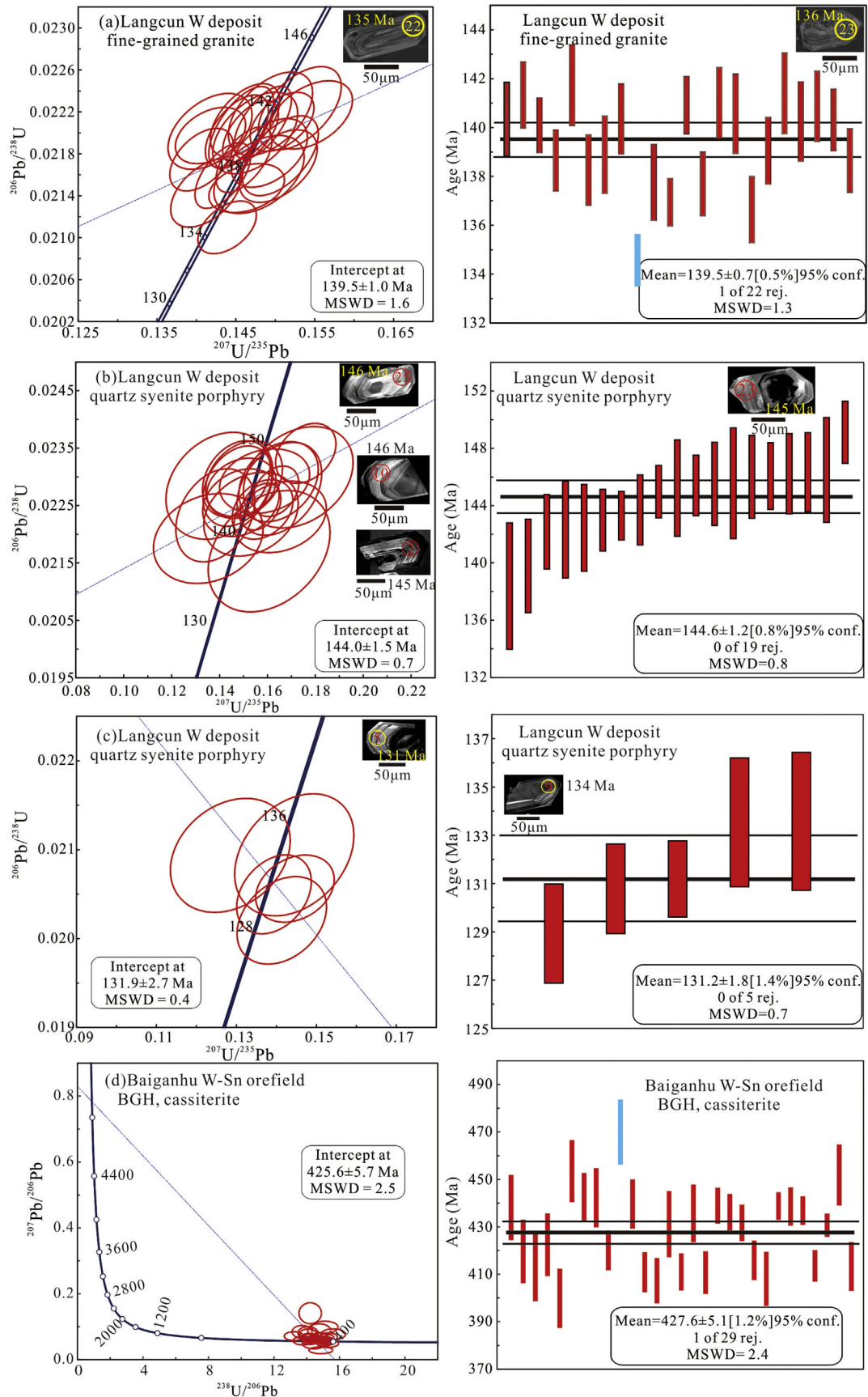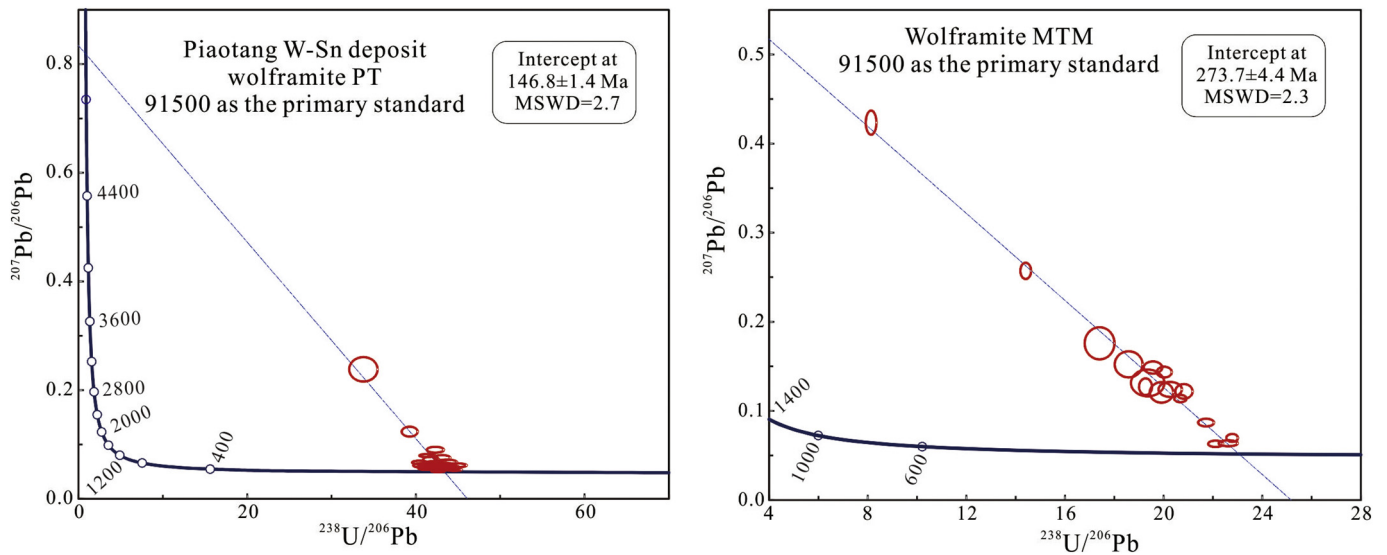
Fig. 5. LA-ICP-MS U—Pb concordia diagrams and histograms of weighted average ages for the analyzed zircon grains in fine-grained granite and granite porphyry from the Langcun W deposit (a-c) and Tera-Wasserburg plots, lower intercept and weighted mean ages of cassiterite from the Baiganhu ore district (d).

Fig. 6. Tera-Wasserburg plots and the lower intercepts ages of wolframite samples of PT (from the Piaotang deposit) and MTM (using 91500 as primary standard for calibration of Pb—Pb and U—Pb ratios).

China (Li et al., 2013c; Lv et al., 2017 and the reference therein), accompanied with coeval I- and S-type granites (Table 3). However, intrusion-associated W-Cu-Mo-Pb-Zn-Sn mineralization during this period have not been well studied, e.g., only the ages of the Xianglushan and Jinzhuping deposits were collected when Mao et al. (2011) described the mineralization events between 140 and 120 Ma in the QHMB. Moreover, due to lack of coeval magmatic event, two relatively isolated ages of 134.7 ± 3.5 Ma for the Fozichong and 138.7 ± 2.7 Ma for the Tieshajie were difficult to be interpreted (Luo et al., 2012; Wang et al., 2013). Recently, more than ten of reliable mineralization ages were reported and ranged mainly from 140 to 120 Ma (Table 3), which are coeval with the time of magmatic events in the NE QHMB. The mineralization ages of the Anji Gangkou polymetallic (137 Ma), Taizishan-Fuling W-Cu-Mo (135 Ma), Huangbi Pb—Zn (135–139 Ma), Jinzhuping Pb-Zn-Mo (135.5 Ma) and Wangwu Mo—Cu (135 Ma) (Table 3) also offer the clues that the mineralization ages of the Fozichong and Tieshajie deposits are reliable, and in combination of the S, Pb and O—H isotopic data of these two deposits we have collected before (Tang et al., 2017b), we conclude that they are most likely intrusion-related. Moreover, in situ wolframite and cassiterite U—Pb chronology by LA-ICP-MS was developed and applied to directly dating the W and Sn mineralization. Thus, two ages of 127.4 ± 4.8 Ma for the Langcun W deposit and 128.3 ± 2.5 for the Jianfengpo Sn deposit are obtained and coeval with the Molybdenite Re—Os age of 125.5 Ma for the large-size Xianglushan W deposit (Table 3), confirming that there exists an important W—Sn mineralization event in this period in South China. Summarily, the close temporal and spatial relationships indicate that these A-, I- and S-type granites and W-Cu-Mo-Pb-Zn-Sn mineralization may have the genetic relationship with each other and are resulted from the same tectonic-magmatic-hydrothermal events in South China. Thus, detail studies on both of them could provide important clues for understanding this special Late Jurassic-Early Cretaceous tectonic environment.

6. Conclusions

1) Wolframite sample of MTM shows inhomogeneous in different grains, most of which contain considerable and variable common lead and are not suitable as the primary standard material for wolframite U—Pb dating using the normal normalization method as zircons.
2) Robust age can be determined for W mineralization by LA-ICP-MS U—Pb dating of wolframite using NIST612 or 614 and MTM as a primary standard for calibration of Pb—Pb and U—Pb ratios, respectively.
3) Directly dating of metal minerals for the Langcun W, Jianfengpo Sn and large-size Xianglushan W deposits confirm that there exists an important W—Sn mineralization event in 125–130 Ma.
4) In South China, during 140 to 120 Ma, A-, I- and S-type granites and W-Cu-Mo-Pb-Zn-Sn mineralization may have a genetic relationship with each other and are resulted from the same tectonic-magmatic-hydrothermal events.

Supplementary data to this article can be found online at https://doi.org/10.1016/j.gr.2020.02.006.

CRediT authorship contribution statement

Yanwen Tang: Conceptualization, Methodology, Supervision, Validation, Formal analysis, Investigation, Writing - original draft, Writing - review & editing, Data curation, Visualization, Funding acquisition. **Kai Cui:** Resources, Methodology, Writing - review & editing. **Zhen Zheng:** Resources, Writing - review & editing, Funding acquisition. **Jianfeng Gao:** Writing - review & editing. **Junjie Han:** Validation. **Jiehua Yang:** Resources, Methodology, Writing - review & editing, Funding acquisition. **Liang Liu:** Methodology, Writing - review & editing, Funding acquisition.

Declaration of competing interest

The authors declare that they have no known competing financial interests or personal relationships that could have appeared to influence the work reported in this paper.
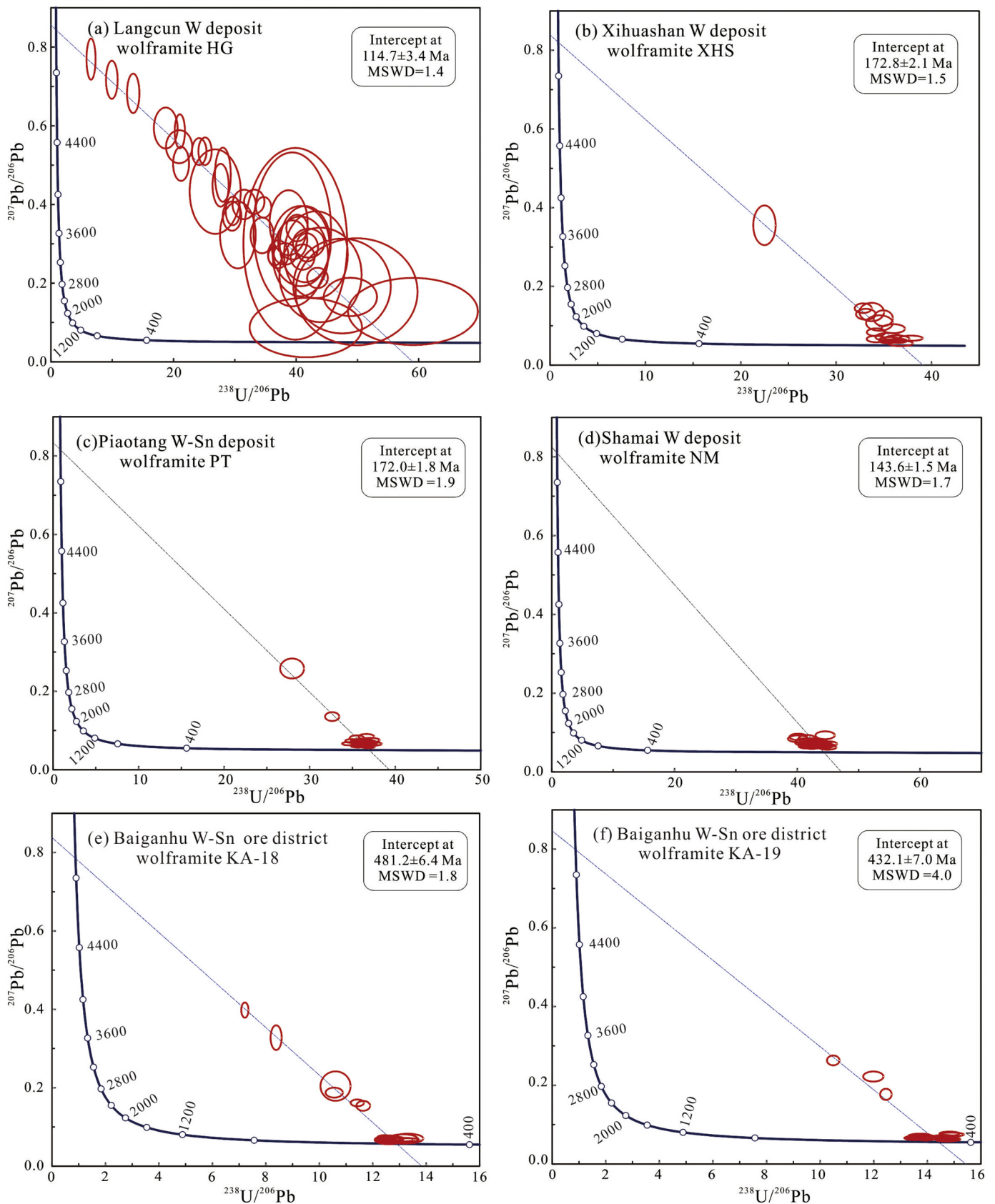
Acknowledgments

Fig. 7. Tera-Wasserburg plots and the lower intercepts ages of wolframite samples from the Langcun, Xihuashan, Piaotang, Shamai W (Sn) deposits and the Baiganhu W (Sn) ore district (using the nearly concordant MTM spots as primary standards for calibration of Pb—Pb and U—Pb ratios).

Table 3
The ages of late Jurassic-early Cretaceous intrusive rocks and associated mineralization in South China.

Ore deposit	Metal association and deposit type	Intrusive rocks	Timing of intrusion (Ma)	Intrusion associated with mineralization	Mineralization age (Ma)	Reference
Anji Langcun W deposit	W-Mo Porphyry-skarn	I- and A-type, Complex	Zircon LA–ICP-MS U—Pb 144.6 ± 1.2–131.2 ± 1.8	Granite porphyry, 131.2 ± 1.8 Ma	Wolframite U—Pb, 127.4 ± 4.8 Ma	This paper
Anji polymetallic deposit	Fe-Zn-Cu, Pb-Zn-Ag-Cu, and Mo Skarn-porphyry	I-type, Complex	Zircon LA–ICP-MS U—Pb 150.2 ± 1.3–139.2 ± 1.2(Certified by 91,500)	Fine-grained granite 139.2 ± 1.2	Molybdenite Re—Os, 139 ± 5; Garnet U—Pb, 137 Ma	Xie et al., 2012; Tang et al., 2012, 2013 and our new geochronology study
Zhuxiling W deposit	W-Mo Skarn-porphyry	I-type, Granite	Zircon LA–ICP-MS U—Pb 138 ± 1.3–142.4 ± 1.6	Granite	Molybdenite Re—Os, 140.2 ± 1.5	Chen et al., 2013b; Kong et al., 2018
Mugua W-Mo-Bi mineralization	W-Mo-Bi Greisen type	S-type, Granite porphyry	Zircon LA–ICP-MS U—Pb 142.2 ± 1.2	Granite porphyry	No report	Li et al., 2013c; Jin and An, 2016
Taizishan, Fuling W—Cu, Mo mineralization	W-Cu, Mo Porphyry	A-type, Complex	Zircon LA–ICP-MS U—Pb 133.9 ± 1.1–129.9 ± 0.7	Granite	Molybdenite Re—Os, 134.6 ± 3.5	Zhang et al., 2005; Chen et al., 2013a; Wan et al., 2018
Jianfengpo Sn deposit	Sn Skarn	I-type, Granite	Zircon SHRIMP U—Pb 128 ± 1–129 ± 2	Granite	Cassiterite U—Pb, 128.3 ± 2.5	Xu et al., 2015, 2017
Lishanling Cu Deposit	Cu Porphyry	S-type, Granite porphyry	Zircon SHRIMP U—Pb 131 ± 2	Granite porphyry	No report	Wang et al., 2016
Huangbi Pb—Zn deposit	Pb-Zn magmatic-hydrothermal type	Basic rock	No report	Basic rock	Sphalerite Rb—Sr and Sm—Nd, 139 ± 15 and 135.4 ± 4.4	Zhang et al., 2012
Jinzhuping Pb-Zn-Mo deposit	Pb-Zn-Mo magmatic-hydrothermal type	Granite	No report	Granite	Molybdenite Re—Os, 135.5 ± 5.7	Zhang et al., 2009
Xianglushan W deposit	W Skarn	Biotite granite	Zircon LA–MC–ICP-MS U—Pb 123.8 ± 0.8	Biotite granite	Molybdenite Re—Os, 125.5 ± 0.7; Ar—Ar dating, 122.8 ± 0.78	Dai et al., 2018a
Wangwu Mo—Cu deposit	Mo-Cu Porphyry	Granite porphyry	Zircon LA–ICP-MS U—Pb 136.7 ± 2.2–130.3 ± 1.1	Granite porphyry	Molybdenite Re—Os, 134.8 ± 2.1	Dai et al., 2018b
Dahutang W deposit(stage III and IV)	W deposit magmatic-hydrothermal type	S-type, Complex	Zircon LA–ICP-MS U—Pb 144.0 ± 0.6–130.3 ± 1.1	Late granites	Molybdenite Re—Os, 141.0 ± 1.2–130.4 ± 1.9	Huang and Jiang, 2014; Song et al., 2018
Fozichong	Pb-Zn-Cu Skarn Cu	Not clear	Not clear	Not clear	Sephalerite Rb—Sr 134.7 ± 3.5?	Luo et al., 2012
Tieshajie	SEDEX or magmatic-hydrothermal type?	Not clear	Not clear	Not clear	K-fildspar Ar—Ar 138.7 ± 2.7	Wang et al., 2013

References

Aleinikoff, J.N., Wintsch, R.P., Tollo, R.P., Unruh, D.M., Fanning, C.M., Schmitz, M.D., 2007. Ages and origins of rocks of the Killingworth dome, south-central Connecticut: Implications for the tectonic evolution of southern New England. Am. J. Sci. 307, 63–118.

Black, L.P., Kamo, S.L., Allen, C.M., Davis, D.W., Aleinikoff, J.N., Valley, J.W., Mundil, R., Campbell, I.H., Korsch, R.J., Williams, I.S., Foudoulis, C., 2004. Improved ²⁰⁶Pb/²³⁸U microprobe geochronology by the monitoring of a trace-element-related matrix effect; SHRIMP, ID-TIMS, ELA–ICP–MS and oxygen isotope documentation for a series of zircon standards. Chem. Geol. 205, 115–140.

Burn, M., Lanari, P., Pettke, T., Engi, M., 2017. Non-matrix-matched standardisation in LA-ICP-MS analysis: general approach, and application to allanite Th–U–Pb dating. J. Anal. At. Spectrom. 32, 1359–1377.

Chen, F., Wang, D.H., Du, J.G., Xu, W., Hu, H.F., Yu, Y.L., Tang, J.L., 2013a. New dating of the fuling granite body with LA-ICP-MS zircon U-Pb in Jixi, Anhui province and their geological significance. Rock and Mineral Analysis 32, 970–977 (in Chinese with English abstract).

Chen, Q., 2015. Simply discussion on the prospecting condition and prospecting direction of Langcun deposit. Annual Meeting of Zhejiang Geological Society 2015, 99–104 (in Chinese with English abstract).

Chen, S.Q., 2011. Discussion on the Yanshan Epoch Rock Characteristics and Ore–Forming Background in Zhejiang Kaihua Region. China University of Geosciences, pp. 18–40 (Paper for Master's Degree, In Chinese with English abstract).

Chen, X.F., Wang, Y.G., Sun, W.D., Yang, X.Y., 2013b. Zircon U-Pb chronology, geochemistry and genesis of the Zhuxiling granite in Ningguo, Southern Anhui. Acta Petrol. Sin. 87, 1662–1678 (in Chinese with English abstract).

Cheng, Y.B., Spandler, C., Kemp, A., Mao, J.W., Rusk, B., Hu, Y., Blake, K., 2019. Controls on cassiterite (SnO₂) crystallization: evidence from cathodoluminescence, trace-element chemistry, and geochronology at the Gejiu Tin District. Am. Mineral. 104, 118–129.

Chew, D.M., Sylvester, P.J., Tubrett, M.N., 2011. U–Pb and Th–Pb dating of apatite by LA-ICPMS. Chem. Geol. 280, 200–216.

Chew, D.M., Petrus, J.A., Kamber, B.S., 2014. U–Pb LA–ICPMS dating using accessory mineral standards with variable common Pb. Chem. Geol. 363, 185–199.

Coogan, L.A., Parrish, R.R., Roberts, N.M., 2016. Early hydrothermal carbon uptake by the upper oceanic crust: Insight from in situ U-Pb dating. Geology 44, 147–150.

Dai, P., Mao, J., Wu, S., Xie, G., Luo, X., 2018a. Multiple dating and tectonic setting of the Early Cretaceous Xianglushan W deposit, Jiangxi province, south China. Ore Geol. Rev. 95, 1161–1178.

Dai, P., Wu, S.H., Ding, C.W., 2018b. Zircon U-Pb dating of granite porphyry and Re-Os isotopic dating of molybdenite from Wangwu porphyry Mo-Cu deposit, Jiangxi Province, and their geological significance. Acta Petrol. Sin. 34, 2598–2614 (in Chinese with English abstract).

Deng, X.D., Luo, T., Li, J.W., Hu, Z.C., 2019. Direct dating of hydrothermal tungsten mineralization using in situ wolframite U–Pb chronology by laser ablation ICP-MS. Chem. Geol. 515, 94–104.

Feng, C.Y., Li, G.C., Li, D.X., Zhou, A.S., Li, H.M., 2013. Ore-controlling structure and ⁴⁰Ar/³⁹Ar geochronology of Kekekaerde tungsten-tin deposit in Qimantage area, Xinjiang. Mineral Deposits 32, 207–216 (in Chinese with English abstract).

Gao, Y.B., Li, W.Y., Li, Z.M., Wang, J., Hattori, K., Zhang, Z.W., Geng, J.Z., 2014. Geology, geochemistry, and genesis of tungsten-tin deposits in the Baiganhu district, Northern Kunlun Belt, northwestern China. Econ. Geol. 109, 1787–1799.

Godeau, N., Deschamps, P., Guihou, A., Guihou, A., Leonide, P., Tendil, A., Gerdes, A., Hamelin, B., Girard, Jean-P, 2018. U-Pb dating of calcite cement and diagenetic history in microporous carbonate reservoirs: case of the Urgonian limestone, France. Geology 46, 247–250.

Gonçalves, G.O., Lana, C., Scholz, R., Buick, I.S., Gerdes, A., Kamo, S.L., Corfu, F., Marinho, M.M., Chaves, A.O., Valeriano, C., Nalini Jr., H.A., 2016. An assessment of monazite from the Itambé pegmatite district for use as U–Pb isotope reference material for microanalysis and implications for the origin of the "Moacyr" monazite. Chem. Geol. 424, 30–50.

Guo, J., Zhang, R.Q., Sun, W.D., Ling, M.X., Hu, Y.B., Wu, K., Luo, M., Zhang, L.C., 2018. Genesis of tin-dominant polymetallic deposits in the Dachang district, South China:

Insights from cassiterite U–Pb ages and trace element compositions. Ore Geol. Rev. 95, 863–879.

Harlaux, M., Romer, R.L., Mercadier, J., Morlot, C., Marignac, C., Cuney, M., 2018. 40 Ma of hydrothermal W mineralization during the Variscan orogenic evolution of the French Massif Central revealed by U–Pb dating of wolframite. Mineral. Deposita 53, 21–51.

Hu, R.Z., Wei, W.F., Bi, X.W., Peng, J.T., Qi, Y.Q., Wu, L.Y., Chen, Y.W., 2012. Molybdenite Re–Os and muscovite $^{40}Ar/^{39}Ar$ dating of the Xihuashan tungsten deposit, central Nanling district, South China. Lithos 150, 111–118.

Hu, Z.C., Gao, S., Liu, Y.S., Hu, S.H., Chen, H.H., Yuan, H.L., 2008. Signal enhancement in laser ablation ICP-MS by addition of nitrogen in thecentral channel gas. J. Anal. At. Spectrom. 23, 1093–1101.

Huang, L.C., Jiang, S.Y., 2014. Highly fractionated S-type granites from the giant Dahutang tungsten deposit in Jiangnan Orogen, Southeast China: geochronology, petrogenesis and their relationship with W-mineralization. Lithos 202-203, 207–226.

Jia, D.L., Yan, G.S., Ye, T.Z., Pang, Z.S., Li, Y.S., He, P.F., Yao, L., Liu, P., 2013. Zircon U-Pb dating, Hf isotopic compositions and petrochemistryof the Guangshan granitic complex in Shaoxing area of Zhejiang province and its geological significance. Acta Petrol. Sin. 29, 4087–4103.

Jiang, S.H., Bagas, L., Hu, P., Han, N., Chen, C.L., Liu, Y., Kang, H., 2016. Zircon U–Pb ages and Sr–Nd–Hf isotopes of the highly fractionated granite with tetrad REE patterns in the Shamai tungsten deposit in eastern Inner Mongolia, China: implications for the timing of mineralization and ore genesis. Lithos 261, 322–339.

Jin, B., An, Z., 2016. Genesis and geological characteristics of Mugua W-Bi deposit in Chun'an country, Zhejiang province, China. Xinjiang Nonferrous Metals 2, 57–59 (in Chinese).

Kennedy, A.K., Kamo, S.L., Nasdala, L., Timms, N.E., 2010. Grenville skarn titanite: potential reference material for SIMS U–Th–Pb analysis. Can. Mineral. 48, 1423–1443.

Kong, Z.G., Liang, T., Mao, J.W., Xu, S.F., Xu, H.B., Yan, P.P., Jin, X.Y., 2018. Study on perogenesis of granodiorite, metallogenic epoch and petrogenetic-metallogenetic setting in the Zhuxiling tungsten polymetallic deposit, southern Anhui province, China. Acta Petrol. Sin. 34, 2632–2656 (in Chinese with English abstract).

Lapierre, H., Jahn, B.M., Charvet, J., Yu, Y.W., 1997. Mesozoic felsic arc magmatism and continental olivine tholeiites in Zhejiang Province and their relationship with the tectonic activity in southeastern China. Tectonophysics 274, 321–338.

Li, C.Y., Zhang, R.Q., Ding, X., Ling, M.X., Fan, W.M., Sun, W.D., 2016b. Dating cassiterite using laser ablation ICP-MS. Ore Geol. Rev. 72, 313–322.

Li, G.C., Feng, C.Y., Wang, R.J., Ma, S.C., Li, H.M., Zhou, A.S., 2012a. SIMS zircon U-Pb age, petrochemistry and tectonic implications of granitoids in northeastern Baiganhe W–Sn orefield, Xinjiang. Diqiu Xuebao. Acta Geosci. Sin. 33, 216–226 (in Chinese with English abstract).

Li, J.J., Fu, C., Tang, W.L., Li, H.M., Lin, Y.X., Zhang, T., Wang, S.G., Zhao, Z.L., Dang, Z.C., Zhao, L.J., 2016a. The metallogenic age of the Shamai wolframite deposit in Dong Ujimqin Banner, Inner Mongolia. Geol. Bull. China 35, 524–530 (in Chinese with English abstract).

Li, Q.L., Li, X.H., Wu, F.Y., Yin, Q.Z., Ye, H.M., Liu, Y., Tang, G.Q., Zhang, C.L., 2012b. In-situ SIMS U–Pb dating of phanerozoic apatite with low U and high common Pb. Gondwana Res. 21, 745–756.

Li, Q.L., Li, X.H., Lan, Z.W., Guo, C.L., Yang, Y.N., Liu, Y., Tang, G.Q., 2013a. Monazite and xenotime U–Th–Pb geochronology by ion microprobe: dating highly fractionated granites at Xihuashan tungsten mine, SE China. Contrib. Mineral. Petrol. 166, 65–80.

Li, X.H., Long, W.G., Li, Q.L., Liu, Y., Zheng, Y.F., Yang, Y.H., Chamberlain, K.R., Wan, D.F., Guo, C.H., Wang, X.C., Tao, H., 2010. Penglai zircon megacrysts: a potential new working reference material for microbeam determination of Hf-O isotopes and U-Pb age. Geostand. Geoanal. Res. 34, 117–134.

Li, X.H., Tang, G.Q., Gong, B., Yang, Y.H., Hou, K.J., Hu, Z.H., Li, Q.L., Liu, Y., Li, W.X., 2013b. Qinghu zircon: a working reference for microbeam analysis of U-Pb age and Hf and O isotopes. Chin. Sci. Bull. 58, 4647–4654.

Li, X.H., Liu, X.M., Liu, Y.S., Su, L., Sun, W.D., Huang, H.Q., Yi, K., 2015. Accuracy of LA–ICP–MS zircon U-Pb age determination: an inter-laboratory comparison. Sci. China Earth Sci. 58, 1722–1730.

Li, Z.L., Zhou, J., Mao, J.R., Yu, M.G., Li, Y.Q., Hu, Y.Z., Wang, H.H., 2013c. Age and geochemistry of the granitic porphyry from the northwestern Zhejiang province, SE China, and its geological significance. Acta Petrol. Sin. 29, 3607–3622 (in Chinese with English abstract).

Luo, J.L., Zhang, Y.H., Zhai, L.N., Liu, W., Jiang, H., 2012. The sphalerite Rb–Sr isotopic chronology of Fuzichong Pb–Zn deposit. Geology of Chemical Minerals 34, 26–31 (in Chinese with English abstract).

Luo, T., Deng, X.D., Li, J.W., Hu, Z.C., Zhang, W., Liu, Y.S., Zhang, J.F., 2019. U–Pb geochronology of wolframite by laser ablation inductively coupled plasma mass spectrometry. J. Anal. At. Spectrom. 34, 1439–1446.

Lv, J.S., Zhang, X.H., Sun, J.D., Zhang, Y., Wu, B., Luo, X.Q., 2017. Spatiotemporal evolution and metallogenic regularity of felsic rocks in the Yanshanian of the eastern segment Qinhang metallogenic belt, South China. Acta Petrol. Sin. 33, 3635–3658 (in Chinese with English abstract).

Mao, J.W., Chen, M.H., Yuan, S.D., Guo, C.L., 2011. Geological characteristics of the Qinhang (or Shihang) metallogenic belt in south China and spatial-temporal distribution regularity of mineral deposits. Acta Geol. Sin. 85, 636–658 (in Chinese with English abstract).

Mao, J.W., Cheng, Y.B., Chen, M.H., Pirajno, F., 2013. Major types and time-space distribution of Mesozoic ore deposits in south China and their geodynamic settings. Mineral. Deposita 48, 267–294.

Mcfarlane, C.R.M., 2016. Allanite U-Pb geochronology by 193 nm LA ICP-MS using NIST610 glass for external calibration. Chem. Geol. 438, 91–102.

Nuriel, P., Weinberger, R., Kylander-Clark, A.R.C., Hacker, B.R., Craddock, J.P., 2017. The onset of the Dead Sea transform based on calcite age-strain analyses. Geology 45, 587–590.

Roberts, N.M., Rasbury, E.T., Parrish, R.R., Smith, C.J., Horstwood, M.S., Condon, D.J., 2017. A calcite reference material for LA-ICP-MS U-Pb geochronology. Geochem. Geophys. Geosyst. 18, 2807–2814.

Roberts, N.M.W., Walker, R.J., 2016. U-Pb geochronology of calcite-mineralized faults: absolute timing of rift-related fault events on the northeast Atlantic margin. Geology 44, 531–534.

Romer, R.L., 2001. Lead incorporation during crystal growth and the misinterpretation of geochronological data from low-$^{238}U/^{204}Pb$ metamorphic mineral. Terra Nova 13, 258–263.

Sheng, J.F., Liu, L.J, Wang, D.H., Chen, Z.H., Ying, L.J., Huang, F., Wang, J., Zeng, L., 2015. A preliminary review of metallogenic regularity of tungsten deposits in China. Acta Geograph. Sin. 89, 1359–1374.

Song, W.L., Yao, J.J., Chen, H.Y., Sun, W.D., Lai, C., Xiang, X.K., Luo, X.H., Jourdan, F., 2018. A 20 my long-lived successive mineralization in the giant Dahutang W–Cu–Mo deposit, south China. Ore Geol. Rev. 95, 401–407.

Tang, Y.W., Xie, Y.L., Li, Y.X., Qiu, L.M., Liu, B.S., Li, Y., Zhang, X.X., Jiang, Y.C., Han, Y.D., 2012. Petrogeochemical and petrographic characteristics and genesis of Wushanguan complex body in Anji ore district, Zhejiang province. Mineral Deposits 31, 903–916 (in Chinese with English abstract).

Tang, Y.W., Xie, Y.L., Li, Y.X., Qiu, L.M., Zhang, X.X., Han, Y.D., Jiang, Y.C., 2013. LA–ICP–MS U-Pb ages, geochemical characteristics of the zircons from Wushanguan complex body in Anji mining area, northwestern Zhejiang and their geological significances. Geol. Rev. 59, 702–715 (in Chinese with English abstract).

Tang, Y.W., Li, X.F., Xie, Y.L., Liu, L., Lan, T.G., Meffre, S., Huang, C., 2017a. Geochronology and geochemistry of late Jurassic adakitic intrusions and associated porphyry Mo–Cu deposit in the Tongcun area, East China: Implications for metallogenesis and tectonic setting. Ore Geol. Rev. 80, 289–308.

Tang, Y.W., Xie, Y.L., Liu, L., Lan, T.G., Yang, J.L., Sebastien, M., Yin, R.C., Liang, S.S., Zhou, L.M., 2017b. U–Pb, Re–Os and Ar–Ar dating of the Linghou polymetallic deposit, southeastern China: implications for metallogenesis of the Qingzhou–Hangzhou metallogenic belt. J. Asian Earth Sci. 137, 163–179.

Thompson, J., Meffre, S., Maas, R., Kamenetsky, V., Kamenetsky, M., Goemann, K., Ehrig, K., Danyushevsky, L., 2016. Matrix effects in Pb/U measurements during LA-ICP-MS analysis of the mineral apatite. J. Anal. At. Spectrom. 31, 1206–1215.

USGS, 2019. Tin and tungsten. Mineral Commodity Summaries. 173, p. 179.

Wan, J.J., Wang, A.D., Ding, N., Tao, J.H., Liu, C.D., Li, X.C., Lin, L.F., Li, C., 2018. Re-Os geochronology and S isotope geochemistry of molybdenite from Taizishan ore-bearing pluton, Jixi county, Anhui province, China. Acta Mineral. Sin. 38, 214–222 (in Chinese with English abstract).

Wang, F.Y., Li, C.Y., Ling, M.X., Zhang, H., Sun, Y.L., Sun, W.D., 2011. Geochronology of the Xihuashan tungsten deposit in southeastern China: constraints from Re–Os and U–Pb dating. Resour. Geol. 61, 414–423.

Wang, H.Z., Zhang, D., Di, Y.J., Luo, P., Lv, L.Y., Dong, Y., Lu, J.H., 2013. Hydrothermal potash feldspar Ar–Ar dating for Tieshajie copper deposit, Jiangxi Province. Acta Petrol. Sin. S2, 613–614 (in Chinese).

Wang, K.Q., Zhang, D.H., Zhu, Y.D., Fu, F., Yin, X.B., Wang, C.S., 2016. Petrogenic age and magma source of granite porphyry in Lishanling porphyry Cu deposit in Changshan area, Zhejiang province. J. Jilin Univ. (Earth Sci. Ed.) 46, 736–748 (in Chinese with English abstract).

Wiedenbeck, M., Allé, P., Corfu, F., Griffin, W.L., Meier, M., Oberli, F., Quadt, A.V., Roddick, J.C., Spiegel, W., 1995. Three natural zircon standards for U-Th-Pb, Lu-Hf, trace element and REE analyses. Geostand. Newslett. 19, 1–23.

Wohlgemuth-Ueberwasser, C.C., Jochum, K.P., 2015. Capability of fs-LA-ICP-MS for sulfide analysis in comparison to ns-LA-ICP-MS: reduction of laser induced matrix effects? J. Anal. At. Spectrom. 30, 2469–2480.

Xie, Y.L., Tang, Y.W., Li, Y.X., Qiu, L.M., Liu, B.S., Li, Y., Zhang, X.X., Han, Y.D., Jiang, Y.C., 2012. Petrochemistry, chronology and ore-forming geological significance of fine crystalline granite in Anji polymetallic deposit of Zhejiang province. Mineral Deposits 31, 891–902 (in Chinese with English abstract).

Xie, Y.L., Li, L.M., Li, Y.X., Tang, Y.W., 2015. Porphyry Mo(W)-epithermal Pb, Zn(Ag) Metallogenic System in Dong Ujimqin Qi, Inner Mongolia, China. Geological Publishing House, Beijing, pp. 87–102 (in Chinese).

Xu, B., Jiang, S.Y., Luo, L., 2015. LA-MC-ICP-MS U-Pb dating of cassiterite from the Jianfengpo Sn deposit in the Pengshan Sn-polymetallic ore field, Jiangxi province and its geological significance. Acta Petrol. Sin. 31, 701–708.

Xu, B., Jiang, S.Y., Luo, L., Zhao, K.D., Ma, L., 2017. Origin of the granites and related Sn and Pb-Zn polymetallic ore deposits in the Pengshan district, Jiangxi province, south China: constraints from geochronology, geochemistry, mineral chemistry, and Sr-Nd-Hf-Pb-S isotopes. Mineral. Deposita 52, 337–360.

Yang, J.H., Kang, L.F., Liu, L., Peng, J.T., Qi, Y.Q., 2019. Tracing the origin of ore-forming fluids in the Piaotang tungsten deposit, south China: constraints from in-situ analyses of wolframite and individual fluid inclusion. Ore Geol. Rev. 111, 102939.

Yang, M.G., Mei, Y.W., 1997. Characteristics of geology and metallization in the Qinzhou-Hangzhou paleoplate juncture. Geol. Miner. Resour. South China 52–59 (in Chinese with English abstract).

Yuan, S.D., Peng, J.T., Hao, S., Li, H.M., Geng, J.Z., Zhang, D.L., 2011. In situ LA-MC-ICP-MS and ID-TIMS U–Pb geochronology of cassiterite in the giant Furong tin deposit, Hunan province, south China: new constraints on the timing of tin–polymetallic mineralization. Ore Geol. Rev. 43, 235–242.

Zhang, B.C., He, M.H., Hang, W., Huang, B.L., 2013. Minimizing matrix effect by femtosecond laser ablation and ionization in elemental determination. Anal. Chem. 85, 4507–4511.

Zhang, H., Dai, S.Q., Guan, Y.C., Wu, H.Q., 2005. Petrology and geochemistry of the Fuling mass in Jixi, southern Anhui. Geol. China 32, 411–416 (in Chinese with English abstract).

Zhang, J.J., Wu, M.S., Chen, Z.H., Liu, S.B., Li, L.X., Qiu, L.M., Wu, B., Huang, A.J., Zhu, P.J., 2009. Geochronologic study on the Jinzhuping molybdenum-polymetallic deposit from Shangrao of Jiangxi province. Rock and Mineral Analysis 28, 228–232 (In Chinese with English Abstract).

Zhang, J.J., Wang, D.H., Liu, S.B., Chen, Z.H., Shi, G.H., Wang, J., Wang, Y.Q., Wei, Y.W., 2012. Geochronology and isotopic compositions of the Huangbi lead-zinc deposits, Jiangxi, China. Acta Petrol. Sin. 28, 3325–3333 (In Chinese with English Abstract).

Zhang, R.Q., Lu, J.J., Lehmann, B., Li, C.Y., Li, G.L., Zhang, L.P., Guo, J., Sun, W.D., 2017. Combined zircon and cassiterite U–Pb dating of the Piaotang granite-related tungsten–tin deposit, southern Jiangxi tungsten district, China. Ore Geol. Rev. 82, 268–284.

Zheng, Z., Chen, Y.J., Deng, X.H., Yue, S.W., Chen, H.J., 2016. Muscovite ^{40}Ar/^{39}Ar dating of the Baiganhu W-Sn orefield, Qimantag, East Kunlun Mountains, and its geological implications. Geol. China 43, 1341–1352 (in Chinese with English abstract).

Zhou, M.F., Gao, J.F., Zhao, Z., Zhao, W., 2018. Introduction to the special issue of Mesozoic W-Sn deposits in south China. Ore Geol. Rev. 101, 432–436.

Zhu, Y.D., 2014. Diagenesis and Metallogeny of Ore–bearing Granites in Tongcun Porphyry Mo–Cu Deposit, Zhejiang. China University of Geosciences, Beingjing, pp. 38–48 (paper for doctoral degree, in Chinese with English abstract).